



Research Article

Measuring the effect of fireworks on air quality in Minneapolis, Minnesota



Andres Gonzalez¹  · Adam Boies²  · Jacob Swanson³  · David Kittelson⁴ 

Received: 24 July 2021 / Accepted: 21 March 2022

Published online: 11 April 2022

Published online: 11 April 2022

© The Author(s) 2022, corrected publication 

Abstract

Air quality was measured before, during, and after a 4th of July fireworks display in downtown Minneapolis, Minnesota using a mix of low-cost sensors (CO, CO₂, and NO) for gases and portable moderate cost instruments for particle measurements (PM_{2.5}, lung deposited surface area, and number weighted particle size distributions). Meteorological conditions—temperature, humidity, and vertical temperature profile were also monitored. Concentrations of particles and most gaseous species peak between 10 pm and midnight on July 4th, decrease in the middle of the night but increase again and by between 6 and 7 am reach concentrations as high or higher than during fireworks. This overnight increase is likely due to a temperature inversion trapping emissions. Between 10 pm and midnight on July 4th the measures of particle concentration increase by 180–600% compared to the same period on July 3rd. Particle size distributions are strongly influenced by fireworks, shifting from traffic-like bimodal distributions before to a nearly unimodal distribution dominated by a large accumulation mode during and after. The shape of the size distribution measured during the early morning peak is nearly identical to that observed during fireworks, suggesting that the early morning peak is mainly due to trapped fireworks emissions not early morning traffic. Gaseous species are less strongly influenced by fireworks than particles. Comparing measurements made between 10 pm and midnight on July 4th and the same period on July 3rd, the concentration of CO increases 32% while the CO₂ increases only 2% but increases by another 15% overnight. The NO concentration behaves oddly, decreasing during fireworks, but then recovering the next morning, more than doubling overnight. Our measurements of CO, NO, and PM_{2.5} are compared with those made at the nearest (~ 2 km away) Minnesota Pollution Control Agency Air Monitoring Station. Their NO results are quite different from ours with much lower concentrations before fireworks, a distinct peak during, followed by a strong overnight increase and an early morning peak somewhat similar in shape and concentration to ours. These differences are likely due mainly to malfunction of our low-cost NO sensor. Concentrations of CO and PM_{2.5} track ours within 25% but peak shapes are somewhat different, which is not unexpected given the spatial separation of the measurements.

Supplementary Information The online version contains supplementary material available at <https://doi.org/10.1007/s42452-022-05023-x>.

✉ Andres Gonzalez, gonza817@umn.edu | ¹Department of Civil, Environmental, and Geo-Engineering, University of Minnesota, Minneapolis, MN, USA. ²Department of Engineering, University of Cambridge, Cambridge, UK. ³Department of Integrated Engineering, Minnesota State University Mankato, Mankato, MN, USA. ⁴Department of Mechanical Engineering, University of Minnesota, Minneapolis, MN, USA.



SN Applied Sciences (2022) 4:142 | <https://doi.org/10.1007/s42452-022-05023-x>

Article highlights

- Low-cost and moderate-cost sensors are used to monitor the impact of a 4th of July fireworks display on local air quality.
- Particle concentrations and size are more strongly influenced by fireworks than are concentrations gaseous pollutants.
- Particle size distributions produced by fireworks are distinctly different from those associated with urban traffic sources.

Keywords Fireworks · Air quality · Low-cost sensor · Minneapolis · Particles · Size distribution

1 Introduction

Fireworks can cause short, but extraordinarily high levels of air pollutants [1]. This can be found during Diwali in India [2], United Kingdom Bonfire Night [3], Chinese Spring festival [4, 5], Guy Fawkes celebration in Auckland, New Zealand [6], and new year in the Netherlands [7]. In the United States, every 4th of July fireworks are launched commemorating the declaration of independence.

The pollutants released from fireworks may degrade air quality and negatively impact human health [7–9]. Although pollutants emitted from fireworks are short-lived, fireworks smoke contains high levels of hazardous chemicals [1]. Exposure to air pollution from fireworks may increase the non-cancer risk for children and adults [10], respiratory problems [11], and hospital admissions [12].

There is a high correlation between fireworks and nitrogen dioxide (NO₂) and nitric oxide (NO), together called NO_x [13]. During fireworks, the NO_x concentration might be twice as high as daytime concentrations [14]. During the Diwali festival in Hisar city of India, the concentration of sulfur dioxide (SO₂) was observed to increase tenfold. Fireworks also release carbon dioxide (CO₂) and carbon monoxide (CO) [15]. The particulate mass concentration below 10 mm diameter (PM₁₀) has been observed to increase from two-fold to nearly ten-fold during fireworks [2, 7]. A study using data from 315 air monitoring station in the United States showed that 1-h mean concentrations of particulate mass below 2.5 mm diameter (PM_{2.5}) measured between 8 pm July 4th and 12 am July 5th increased, compared to average concentrations, by 10–20 μg m⁻³ [8]. In another study, measurements conducted during July 4th fireworks showed that PM_{2.5} reached a peak 1-h average concentration of 55 μg m⁻³; 67% higher than background concentrations [5]. Particle size distribution and composition measurements made during the Diwali festival in India showed a relatively broad number weighted size distribution centered at about 100 nm with total number concentration increasing by about 20,000 particles/cm³ compared to non-festival days and significant increases in

water soluble ion concentrations, notably K⁺, Mg²⁺, NH₄⁺, Cl⁻, and NO₃⁻ [16]. Others have observed that fireworks increase both the size of the particles (> 100 nm) and the total particle number concentration [9, 17]. Measurements of fireworks-related chemicals show statistically significant increases in the concentrations of barium, chlorine, copper, magnesium, potassium, and strontium [18].

Low-cost mobile air quality monitoring (LCMAQM) sensors can be a feasible option to measure the air quality during fireworks. The cost is one of the main strengths of LCMAM sensors ranging from \$150 to \$200 each [19]. The Mobile Autonomous Air Quality Sensor box (MAAQSBx) is a device to measure air quality using LCMAQM sensors [19]. The MAAQSBx contains five gas sensors and two particle sensors, and a wireless broadcasting system [19]. There is consistency in the literature regarding the limitations of LCMAQM sensors. For example, temperature and humidity affect the performance and accuracy of LCMAQM [20] and there are cross-sensitivities of LCMAQM sensors with other gases [20]. To assess the impact of temperature, humidity, and cross-sensitivity on the sensor readings, MAAQSBx was calibrated in the field using as reference Minnesota Pollution Control Agency AMS regulatory equipment [19]. The results are shown in the calibration section below.

The aim of this study is to measure the air quality during the release of fireworks on the 4th of July at 10 pm in downtown Minneapolis, Minnesota. The measurements were conducted using LCMAQM sensors as well as some moderate-cost portable sensors. The gases measured were carbon monoxide (CO), carbon dioxide (CO₂), and nitric oxide (NO). The particle measurements were PM_{2.5} and lung deposited surface area (LDSA) [22, 23]. A unique feature of this study is that particle size and number concentration were also measured using a NanoScan SMPS model 3910(TSI).

In the material and methods section, we describe the location and technology of each sensor. Then, the results of the field measurements, including meteorological conditions are presented, followed by the conclusions.

2 Material and methods

2.1 Location and meteorological conditions

Figure 1 shows the location of the MAAQSBox in the Saint Anthony Falls Laboratory, ~ 330 m away from one of the fireworks launch locations in Minneapolis. The fireworks were launched in the Marcy-Holmes neighborhood between Stone Arch Bridge and Central Ave Bridge. The nearest Minnesota Pollution Control Agency (MPCA) air monitoring station (AMS) is approximately 2 km away from the MAAQSBox location. AMS data serve as a reference.

The meteorological parameters included in the fireworks analysis are wind speed and direction, relative humidity, and vertical temperature profile. All meteorological data except vertical temperature is from the AMS. All air quality and meteorological data from the AMS are hourly averages. Vertical temperature profiles were obtained from twice daily radiosonde soundings available from the University of Wyoming Department of Atmospheric Science website. (<http://weather.uwyo.edu/upperair/sounding.html>).

2.2 Sensor technology

2.2.1 Description of the MAAQSBox

The Fig. 2 shows the schematic of the MAAQSBox. It is an autonomous device that houses five gas sensors and two particle sensors, includes hazard protection and thermal conditioning of sample streams, and continuously broadcasts measured concentrations and system status [19]. All the gas sensors are installed in a Flow Sensing Cell Apparatus (FSCA) [19]. The O₃ and NO₂ sensors are not included in this study due to power supply issues. Also, we discarded OPC-N2 PM_{2.5} sensor results because calibration performance was very poor with R² of only 0.4. Instead, we used an external PM_{2.5} instrument instead (See Sect. 2.2.2 for details).

Concentrations of CO and NO are measured by B4 sensors produced by AlphaSense. Each sensor has three sections: a gas chamber and filter, electrochemical cells, and a reservoir of electrolyte solution [24]. In the electrochemical cells section, there are four electrodes: working, reference, counter, auxiliary [25]. An electrochemical reaction produces current between the working electrode and the counter electrode. This current is proportional of the target gas volume concentration [24]. An individual sensor board designed by AlphaSense is used to reduce environmental noise, improving the resolution of the sensors [21]. The outputs of B4 sensors are working electrode (*We*) and the auxiliary electrode (*Ae*) voltages. The CO₂ concentration is

measured with a low-cost non-dispersive infra-red absorption sensor produced by Yoctupuse [26]. The range measurement is between 0 and 10,000 ppm with 1 ppm resolution [27].

The MAAQSBox also included two particle sensors [19]. An OPC-N2 (not used) and a Partector. The Partector (produced by Naneos) measures particles in a size range from 10 nm to 10 μm weighted to approximate the product of particle surface area and inhaled deposition fraction in the alveolar region of the respiratory system. This is called the lung deposited surface area (LDSA) [22, 23]. Particles are charged with a unipolar charger and then pass through a Faraday cage which is connected to an electrometer measuring the charge transferred to the particles which is proportional to LDSA [28]. The manufacturer gives an operating range of 0–10⁴ mm²/cm³ with an uncertainty of ± 30% and a time response of 4 s. Kuula, et al. [29] used a variety of optical and diffusion-based sensors to measure urban air quality and compare the results with reference measurements in a 1-month test campaign. They found very good agreement between Partector measurements and reference measurements of LDSA calculated from size distributions measured using a Differential Mobility Particle Sizer (6 to 800 nm range). The regression line of Partector versus reference LDSA had a slope of 0.99, intercept of 2.5 mm²/cm³, R² of 0.97 and RMS error of 4.3 mm²/cm³ in the concentration range 0–120 mm²/cm³. Consistent and reliable measurements were made for concentrations as low as 2 mm²/cm³. Our Partector was tested and calibrated by Naneos shortly before beginning this study.

2.2.2 External particle sensors

A TSI SidePak Personal Aerosol Monitor AM510 is a belt mounted laser photometer [30] used to measure PM_{2.5}. The aerosol stream passes through an impactor which removes particles larger than 2.5 μm. Smaller particles continue with the stream into an optical chamber where they are illuminated with a focused beam of laser light at a wavelength of 670 nm [31]. The intensity of scattered light is proportional to the PM_{2.5} concentration [32].

The SidePak is a simple and reliable instrument that gives repeatable measurements for a given aerosol. However, it is a light scattering instrument, and its response depends on particle composition and size. The manufacturer gives a minimum resolution of 1 mg/m³ and an operating range of 1–20 mg/m³. It is factory calibrated with Arizona road dust and has a user adjustable calibration factor (CF) with a value of 1.0 corresponding to factory calibration. Jiang, et al. [31] tested a three AM510s with outdoor urban aerosols and reported mean CFs ranging from 0.66 to 0.93 (measured gravimetric concentration = CF x AM510 reading). They also tested 19 AM510s with aged tobacco

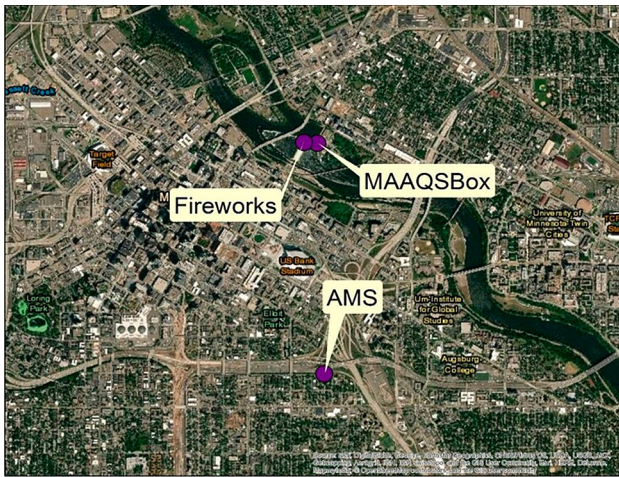


Fig. 1 Location of the firework, measurements (MAAQSBox), and air monitoring station (AMS)

smoke and observed mean CFs in two separate test series of 0.29 and 0.28. In addition, they tested five AM510s on other combustion aerosols: incense CF = 0.35–37, wood chips, CF = 0.77, and toasting bread, CF = 0.79. Wang et al. [33] used an AM510 as reference instrument in an evaluation of low-cost sensors. They also evaluated the response of the AM510 to a variety of aerosols. They did not give results as calibration factors, but CFs may be estimated from slope of their plots of AM510 response versus

standard aerosol concentration. For particles that might be of atmospheric interest, CFs were estimated from their plots to be: 0.22, 0.33, 0.52 and 0.96 for NH_3NO_3 , NaCl, and 600 and 300 nm polystyrene latex particles, respectively. Thus, for many aerosols the AM510 overresponds significantly using the factory calibration but the response is linear and repeatable. We decided to use the factory calibration factor of 1.0 in the absence of better information recognizing that this would likely lead to overestimating absolute concentrations but would allow reasonable estimates of relative concentrations.

The TSI NanoScan SMPS model 3910 is a particle size spectrometer that measures particle concentrations classified by electrical mobility diameter in the range from 9 to 420 nm [34]. The NanoScan contains four main components: a cyclone pre-conditioner to remove coarse particles, a particle charger, a differential mobility size selector, and a particle counter [35, 36]. It is a scanning instrument and requires 1 min to complete a size distribution measurement. Tritscher [34] compared the NanoScan SMPS with a TSI SMPS sizing reference system using several monodisperse and polydisperse test aerosols. It was also tested for linearity against a TSI 3776 ultra-fine CPC as a number concentration reference. In addition, it was also tested in on-road measurements during a freeway journey and in a production test facility. The NanoScan SMPS measurements compared very well with that of the reference SMPS. It also demonstrated linearity with the CPC for

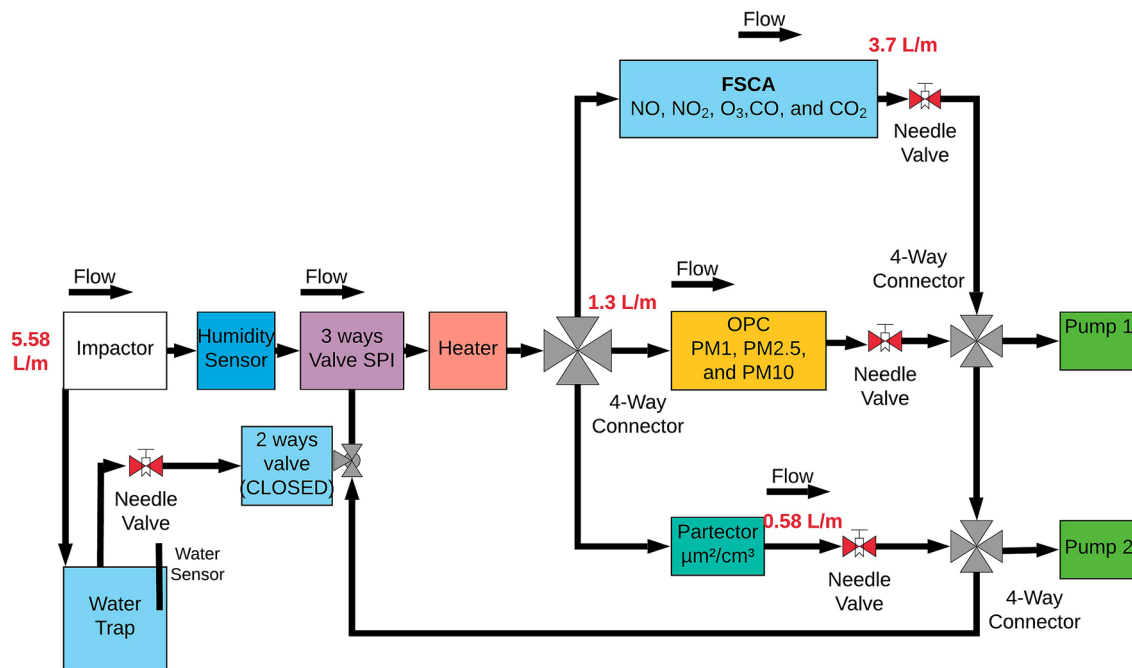


Fig. 2 Schematic of The mobile autonomous air quality sensor box (MAAQSbox)

concentrations as high as 10^6 particles/cm³. TSI reports a usable concentration range for the instrument of 100– 10^6 particles/cm³.

2.3 MAAQSBox field calibrations

The aim of the field calibrations was to evaluate LCMAQM sensor performance compared to reference instruments in the field [19]. The calibrations were conducted with the assistance of the Minnesota Pollution Agency (MPCA). The MAAQSbox was placed next to the same MPCA AMS referenced above. The sensors in the AMS are Teledyne T200 NO_x for NO and NO₂, and T300 for CO. We performed a regression by minimizing the sum of the squared errors. The variables included are working electrode (*We*) and auxiliary electrode (*Ae*) sensor signals, humidity, and temperature. The p-values of each variable must be < 0.05. The details of each model are presented below.

$$\text{CO [ppm]} = \beta_0 + \beta_1 * We_{\text{COsensor}} + \beta_2 * Ae_{\text{COsensor}} + \beta_3 * T^\circ + \beta_4 * RH.$$

$$\text{NO [ppb]} = \beta_0 + \beta_1 * We_{\text{NOsensor}} + \beta_2 * Ae_{\text{NOsensor}} + \beta_3 * T^\circ + \beta_4 * RH.$$

Where β_0 is the intercept when all independent variables are zero, β_x are the regression coefficients, *We*, *Ae*, *T*[°] is temperature in Celsius, and RH is relative humidity in percent [19].

Two field calibrations were conducted, one in June, before the fireworks study and one in August and September, after the study. Calibration 1 was relatively short, about 100 h, and there was significant scatter in the results. Calibration 2 was much longer, about 500 h, and gave much better results. Tables 1 and 2 summarize the results of the CO and NO calibrations. The details of the coefficients, t-stats, and p-values are in the supplementary information (SI1 and SI2). Fig. SI3 shows CO and NO concentrations calculated using calibration 1 plotted against concentrations calculated using calibration 2. The slopes are 0.94 and 0.67 for CO and NO, respectively, so there is a calibration shift, especially for NO. Such calibration shifts have been reported in other studies with low-cost sensors [20]. As can be seen from Tables 1 and 2, the statistics are much better for calibration 2 and we have used that calibration for this study.

2.4 Measurements and statistical analysis

The measurements at the Saint Anthony Falls Laboratory were conducted from July 3rd at 4 pm to July 5th at 10 am. Results are presented in four sections. First, we assess the wind direction and speed, temperature vertical profile, and humidity. Second, CO₂, LDSA, and total particle number concentration (NanoScan) are presented as 15-min averages. Third, we evaluate the particle size distributions

(NanoScan). Finally, the 1-h average data obtained from MAAQSBox are compared to the 1-h average data from the AMS. AMS data are presented in the same plot in two different ways; hourly average data obtained during the current campaign (AMS-1H) and hourly average AMS data for the same time period, July 3rd to July 5th for the previous two years, 2017 and 2018 (AMS-2Y).

The MAAQSBox CO and NO data were recorded and averaged every 1-min in the Yocto-Board. The CO₂ data were recorded by the Arduino. Humidity, rain, water sensors, and valve positions were recorded by another Arduino board. Concentrations of PM_{2.5}, LDSA, and particle number, and size distributions were stored in each instrument's memory. The data analysis and calibration calculations were performed using Matlab, R, and Excel. The data were downloaded to a laptop, then the 1-h and 15-min averages were calculated using Excel. All the plots were made by R using *ggplot* package. Output voltages from the NO and CO sensors as well as temperature and RH were converted to concentrations using calibration coefficients.

3 Results and discussion

3.1 Meteorological conditions

Meteorological conditions are an important factor influencing local pollutant concentrations [37, 38]. Low wind speed (< 4 km h⁻¹) is frequently associated with high levels of air pollution because it reduces dispersion [39, 40]. Temperature inversion is a layer in the atmosphere across which the temperature increases with height [41]. Temperature inversion increases air pollution on the surface due to stable conditions trapping pollutants [42]. Health effects associated with air pollution is greater at low temperature [43, 44]. Also, there is a strong correlation between concentrations of sulfates, nitrates, and ammonium and high relative humidity (RH) [45, 46].

Meteorological parameters such as wind speed and direction and RH were obtained from AMS before, during, and after the fireworks. Figure 3 shows the details of the wind speed (a) and direction (b), humidity (c), and vertical temperature profile (d). On July 3rd between 5 and 11 pm, the wind direction was from the southeast and the speed was 0.9 km h⁻¹, blowing from the AMS to the MAAQSBox, RH was 70% and there was no temperature inversion. This is shown in SI4. On July 4th between 12 and 10 am, the wind direction was from the southeast with a speed of 1 km h⁻¹, RH was 77% and there was no temperature inversion assuming the same vertical temperature profile as on July 3rd between 5 and 11 pm. On July 4th from 11 am to 4 pm, the wind direction was from the south and southwest and the speed was 2.6 km h⁻¹, RH was 77% and

Table 1 Calibration 1 results of B4 gas sensors

Sensor	N, hours	R ²	SE	RC
CO	100	0.86	0.04 ppm	0.3 ppm-0.7 ppm
NO	96	0.52	3.6 ppb	0.2 ppb- 32.4 ppb

N represents the number of hours of calibration for each sensor in the AMS

R² is the coefficient of determination. SE is the standard error

RC represents the range of the concentration during the calibration

Table 2 Calibration 2 results of B4 gas sensors

Sensor	N, hours	R ²	SE	RC
CO	515	0.95	0.02 ppm	0.25 ppm-1.1 ppm
NO	509	0.79	3.1 ppb	1.3 ppb- 46.4 ppb

N represents the number of hours of calibration for each sensor in the AMS

R² is the coefficient of determination

SE is the standard error

RC represents the range of the concentration during the calibration

there was a temperature inversion at 12 pm (SI5). On July 4th from 5 to 11 pm, the wind was from the northwest and the speed was 1.7 km h⁻¹. The fireworks were launched at 10 pm, therefore the wind was from the fireworks to the MAAQSBox and AMS at low speed. The RH was 72% and there was a temperature inversion at ~ 1,000 m (Fig. 3 d) at 12am on July 5th. On July 5th between 12 and 10 am, the wind direction was mainly from the north and the speed was 0.6 km h⁻¹, RH was 83% and temperature inversion was at ~ 300 m at 12 pm (SI6) on July 5th. These conditions limited the dispersion and mixing fluxes. There was no rain during the fireworks launch.

3.2 CO₂ and nanoparticles

The concentrations of CO₂, LDSA, and NanoScan total particle number are plotted in Fig. 4a–b. The concentrations are presented as 15-min averages. The CO₂ concentration in an urban area is strongly correlated with traffic flow [47], time of day, inversion conditions, and wind speed and direction [48]. The average CO₂ concentration between 10 pm on July 4th and midnight on July 5th was only 2% higher compared to the same period the previous night. Thus, there was no immediate impact of the fireworks on the CO₂ concentration. However, the CO₂ concentration began increasing at around 6 pm on July 4th and continued to increase overnight, reaching a peak value of 470 ppm at 6:45 am on July 5th. This behavior is consistent with overnight trapping pollutants by a temperature

inversion. Similar behavior has been observed in other studies [49–54], with peaks ranging from 430 to 450 ppm [52, 55].

Total particle number concentration is calculated by integrating the NanoScan size distribution over the measurement range (9–420 nm). Typically, nearly all the particle number in urban areas is in particles smaller than 500 nm [56], mainly within the NanoScan measurement range. The average LDSA and total particle number concentrations between 10 pm and midnight on July 4th are 30 μm² cm⁻³ and 11,100 particles cm⁻³ for LDSA and number, respectively, compared to 10.6 μm² cm⁻³ and 4,800 particles cm⁻³ the previous night, 220% and 180% higher, respectively. Other particle number concentration measurements conducted during fireworks range from 10,000 cm⁻³ to 100,000 cm⁻³ [16, 57]. The LDSA and number concentrations show additional peaks between 6 and 9 pm on July 3rd, 7 am and 1 pm on July 4th, and 9 pm on July 4th, and 9 am on July 5th. The two later peaks are the highest. These peaks are likely associated with traffic emissions [58, 59]. The average LDSA and number concentrations between 5 and 9 am on July 5th were 140% and 90% higher, respectively, compared to the previous morning. This can be explained by stable environmental conditions that morning (Fig. 3 d and SI6) trapping emissions from fireworks, and morning traffic flow. LDSA and number concentrations are strongly correlated with a coefficient of determination, r² of 0.94 for the period from the entire measurement period.

3.3 Particle size distribution

It is well known that atmospheric aerosols display several distinct size modes linked to formation mechanisms, not rigid size boundaries [56, 60–62]. Typically, there are 3 or 4 distinct modes. There are 2 modes in the so-called ultrafine range currently defined as particles smaller than 100 nm, a nucleation mode below about 10 nm and an Aitken mode between about 10 and 50–100 nm. The nucleation mode consists of particles/molecular clusters freshly formed by nucleation of low vapor pressure species and the Aitken mode consists of larger particles formed by either more intense nucleation events or condensational growth of nucleation mode particles. However, the nucleation and Aitken modes are often merged into a single mode called the nucleation mode. There are 2 larger modes, the accumulation mode formed by condensation and coagulation typically between about 50–100 nm and 500–1000 nm, and a coarse mode formed by mechanical processes typically above about 500–1000 nm diameter. Particle in the nucleation and Aitken modes are short-lived and quickly grow into the accumulation mode range or are lost by evaporation or diffusion. Thus, the highest concentrations

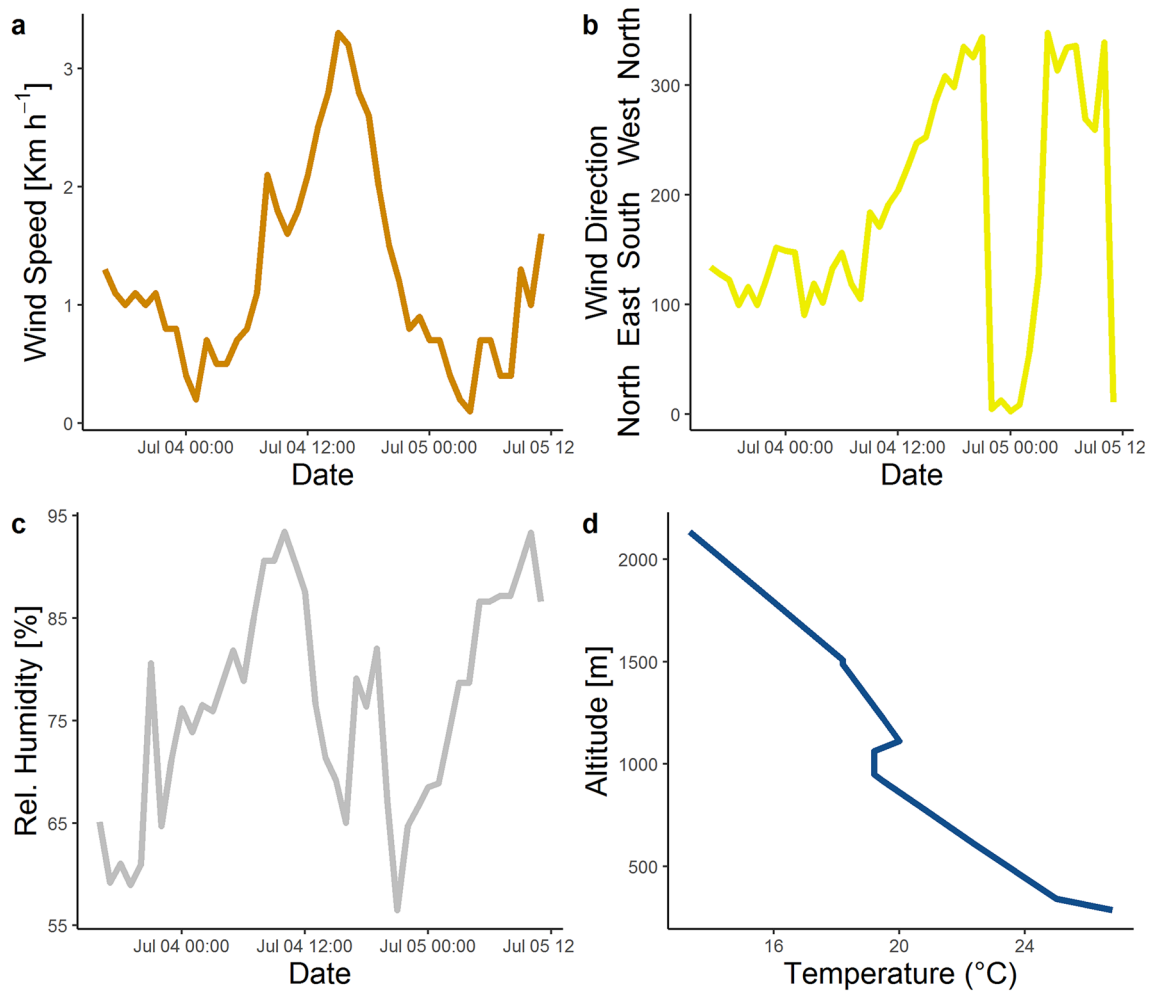


Fig. 3 **a** Wind speed from July 3rd to 5th July. **b** Wind direction from July 3rd to 5th July. **c** The relative humidity from July 3rd to 5th July. **d** Temperature profile on July 5th at 12 am. X-axis is the

temperature in Celsius. The Y-axis is the altitude in meters. Source: data from the University of Wyoming Dept of Atmospheric Science website (<http://weather.uwyo.edu/upperair/sounding.html>)

of these particles are found near the source and decay downwind.

Figure 5a shows number weighted particle size distributions measured at four times: 7 pm on July 3rd and 8 am on July 4th – before fireworks, and 12 and 6 am on July 5th – after fireworks. Averaging times are 115, 155, 152, and 105 min, respectively. The size distributions measured before fireworks show a distinct bimodal structure with a single large nucleation mode peaking between about 25 and 40 nm and a less distinct accumulation modes between about 100 and 150 nm. These modes are like those observed for aged traffic aerosols [56]. During and after fireworks the modes shift dramatically with small nucleation modes peaking around 15 nm and large accumulation modes peaking around 90 nm diameter appearing. The near disappearance of a distinct nucleation mode is likely due to scavenging of nucleation mode particles by coagulation with particles in the large accumulation

mode [56, 63]. The mode shapes are essentially the same at 12 am and 6 am and the concentration is slightly higher at 6 am more than 6 h after the fireworks. This is consistent with the inversion and trapping phenomena described above. Yadav et al. [16] reported very similar size distributions during fireworks at the Diwali festival in 2016 but did not see clearly bimodal traffic aerosols before and after fireworks. On the other hand, Wehner et al. [64] observed a very similar size distribution to ours during millennium fireworks 2000 in Leipzig and also observed distinct bimodal traffic size distributions before and after fireworks.

Figure 5b shows time series plots of the particle number concentrations in the nucleation and accumulation mode size ranges. Although the size distributions do not show clear division between the modes, we have assigned particles smaller than 50 nm to the nucleation mode and particles larger to the accumulation mode, consistent with what is often observed with traffic aerosols. Other studies

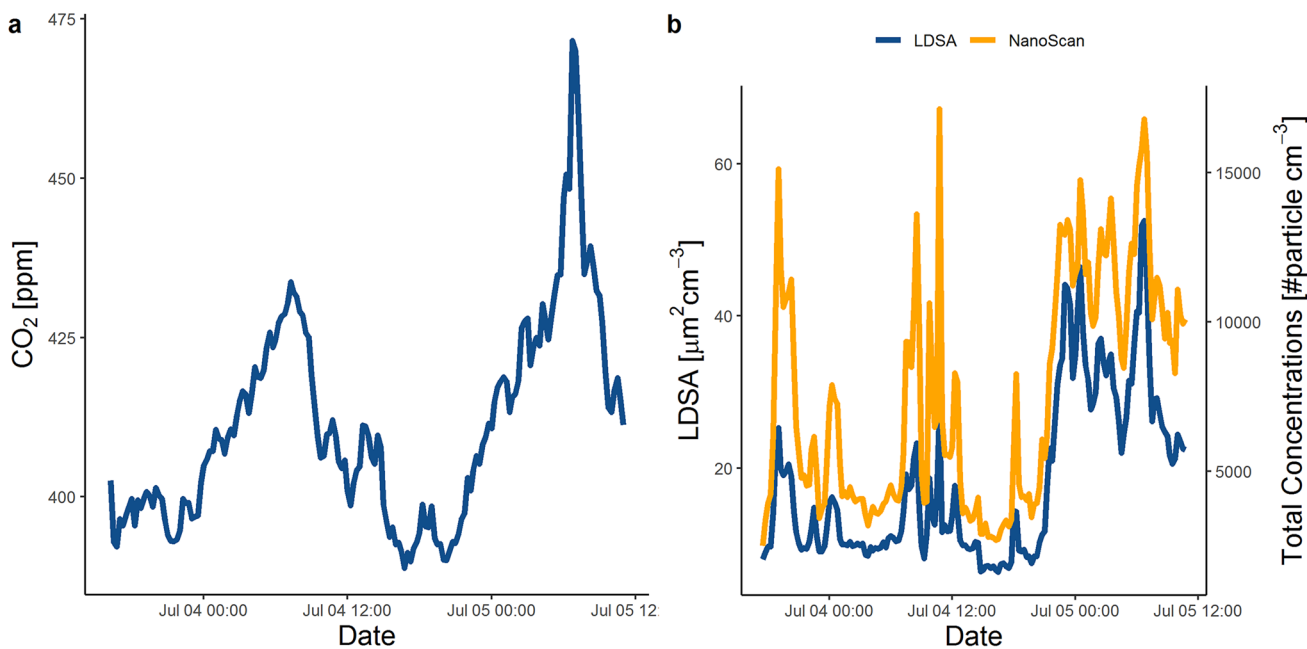


Fig. 4 Concentrations of CO₂, LDSA and total particle number before, during, and after fireworks. **a** CO₂ concentration in ppm. **b** The blue line represents the lung deposited surface area (LDSA)

and the orange line is the total number concentration of particles between 9 and 420 nm. The data are presented as 15 min-averages

have associated fresh traffic emissions with the nucleation mode [65–67]. The accumulation mode often follows the traffic, but it has lower concentrations than the nucleation mode [68, 69]. The highest nucleation mode peaks are at 7 pm on July 3rd with 11,000 particles cm⁻³, and several morning peaks on July 4th ranging from 7,300 to 12,000 particles cm⁻³. These peaks are likely road traffic related. Unlike July 3rd there is no large evening traffic peak on July 4th only reaching 6,000 particles cm⁻³ at 6 pm. Both the nucleation and accumulation mode start to rise at about 9 pm on July 4th but the accumulation mode rises much faster and is dominant during and after the fireworks. The accumulation mode peaks at about midnight and again at about 7 am July 5th reaching 11,000 and 12,000 particles cm⁻³, respectively. The overnight increase is due to the temperature inversions described above (Fig. 3d and S5). Others have observed similar patterns during fireworks [16, 57, 70, 71].

3.4 Fireworks and AMS

The air quality data obtained from MAAQSBox is compared to the air quality from AMS. The AMS data from July 3rd to July 5th are presented in two different ways. First, the AMS hourly averages (AMS-1H) during the same date and time of MAAQSBox. Second, the AMS hourly averages for the same dates and time during the two previous years (AMS-2Y). The data are shown in Fig. 6a–c.

Figure 6a shows that CO measurements of MAAQSBox follow the AMS-1H trend. The data for CO AMS-2Y do not show the normal pattern of variability, likely contain errors, and will not be considered further. The CO concentrations are below 1 ppm and the 8 and 1-h standards are 9 and 35 ppm respectively. The CO concentrations between 10 pm on July 4th and 12 am on July 5th are 0.49 ppm and 0.55 ppm for MAAQSBox and AMS-1H respectively. The MAAQSBox CO concentrations are 32% higher compared with the previous night. A second peak took place between 5 and 9 am on July 5th. The CO concentrations are 0.49 ppm and 0.54 ppm for MAAQSBox and AMS-1H, respectively. During this period there is a temperature inversion, wind speed is less than 0.5 km h⁻¹, and direction is mainly from the northwest.

Figure 6b shows the NO concentrations. The concentrations measured by AMS-1H and AMS-2Y between 12am and 6 pm on July 4th are much lower than concentrations measured by the MAAQSBox during the same time period, < 2 ppb compared to about 6 ppb. However, after 6 pm the AMS-1H and AMS-2Y values rise and show peaks between about 10 pm and midnight, while, on the other hand, the concentration measured by the MAAQSBox falls and reaches a minimum shortly before midnight. Between midnight and about 4 am July 5th, concentrations measured by AMS-1H and AMS-2Y change little and those measured by the MAAQSBox increase slowly, but after 4 am concentrations from AMS-1H and AMS-2Y

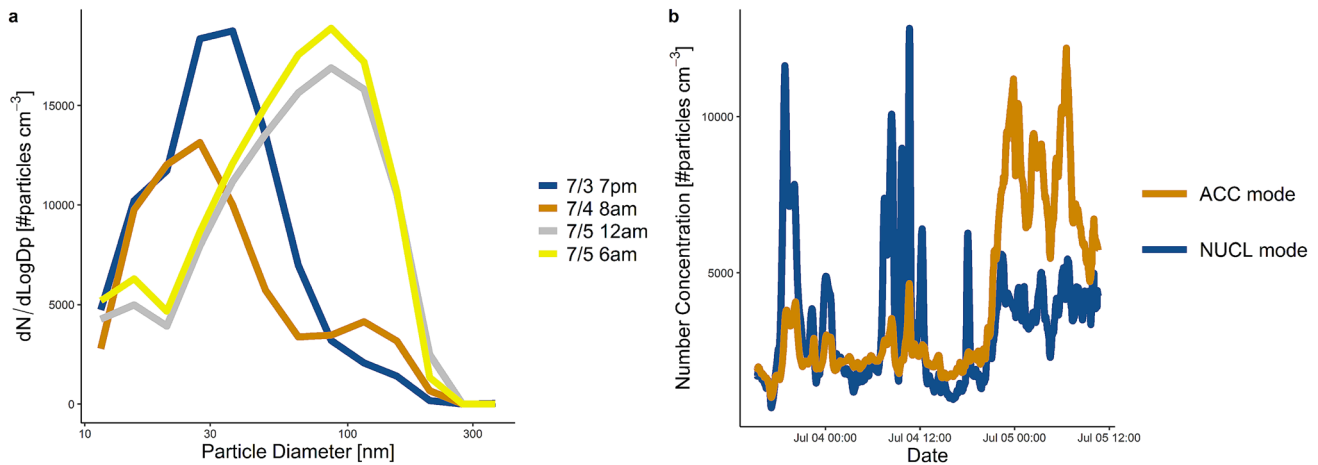


Fig. 5 Fireworks and particle sizes. **a** Number weighted particle size distributions at four times. Blue line represents data at 7 pm on July 3rd, orange line at 8 am on July 4th, grey line at 12 am on July

5th, and yellow line at 7 am on July 5th. **b** Number concentration in particles cm^{-3} classified in two different size ranges. Nucleation mode < 50 nm and accumulation mode > 50 and < 500 nm

and MAAQSBox all rise sharply, peaking at 11 ppb at 6 am and 14 ppb at 7 am, respectively, for the MAAQSBox and AMS-1H. These morning peaks are likely associated with the temperature inversion. These results are puzzling, the difference in behavior between AMS-1H and AMS-2Y and MAAQSBox before 6 pm on July 4th might suggest a malfunction of the NO sensor, but later during the inversion event the AMS-1H and AMS-2Y and MAAQSBox are in reasonable agreement. We do not know the explanation for this. It should be noted the NO is a good marker for fireworks and large peak during a fireworks display is expected. For example, Wehner et al. [64], observed simultaneous sharp peaks in both particle mass and NO concentrations, 240 mg m^{-3} and 14 ppm, respectively, shortly after midnight during the millennium display.

Figure 6c shows that $\text{PM}_{2.5}$ concentrations from AMS-1H and AMS-2Y as well as from the SidePak AM510 monitor. It also shows the accumulation mode number concentration. All concentrations start to rise at about 9 pm on July 4th and peak between about 10 pm and midnight. The accumulation mode number concentration follows the same trend as SidePak $\text{PM}_{2.5}$ mass concentration suggesting that most of the mass is in the accumulation mode. This is typically the case for atmospheric aerosols unless there is a large coarse particle mode [60]. The SidePak $\text{PM}_{2.5}$ concentrations and accumulation mode number concentrations are strongly correlated during the entire measurement period with a coefficient of determination, r^2 of is 0.98. The average $\text{PM}_{2.5}$ concentrations between 10 pm and midnight on July 4th are 63, 45, and $88 \text{ } \mu\text{g m}^{-3}$, for SidePak, AMS-1H, and AMS-2Y respectively. The average accumulation mode number concentration during the same period is $9,100 \text{ particles cm}^{-3}$. The AMS-1H peaks earlier than the SidePak. The SidePak and the AMS

are about 2 km apart so the AMS measurements may be influenced by emissions from other fireworks displays and other sources. Compared to the previous night, $\text{PM}_{2.5}$ concentrations are 500%, 600%, and 520% higher for the SidePak, AMS-1H, and AMS-2Y, respectively and accumulation mode number concentration is 270% higher. Secondary peaks of SidePak $\text{PM}_{2.5}$ and accumulation mode number occur in the morning after fireworks between 6 and 7 am. These peaks are $88 \text{ } \mu\text{g m}^{-3}$ and $10,800 \text{ particles cm}^{-3}$, 40% and 19% higher, for $\text{PM}_{2.5}$ and number, respectively, than during fireworks. Again, this is associated with the temperature inversion (S6) trapping emissions from the fireworks as well as from early morning traffic. Other measurements conducted during fireworks report increases in $\text{PM}_{2.5}$ ranging from $32 \text{ } \mu\text{g m}^{-3}$ to $380 \text{ } \mu\text{g m}^{-3}$ [64, 72–74].

4 Conclusions

We examined the influence of a July 4th fireworks display in downtown Minneapolis on local ambient air quality using low-cost sensors and moderate-cost portable particle instruments and compared these results with measurements made at a nearby (~ 2 km) regulatory air monitoring station (AMS). Portable low-cost and moderate-cost sensors can be deployed more widely than much more expensive AMSs, thus allowing more detailed spatial coverage. The performance of the low-cost sensors was mixed but the particle instruments performed very well.

Low-cost sensors were used to measure CO, CO_2 , and NO. A TSI SidePak, a Naneos Partector, and a TSI NanoScan SMPS were used to measure $\text{PM}_{2.5}$, LDSA, and particle size distributions, respectively. Meteorology data, wind speed and direction, humidity, and vertical temperature

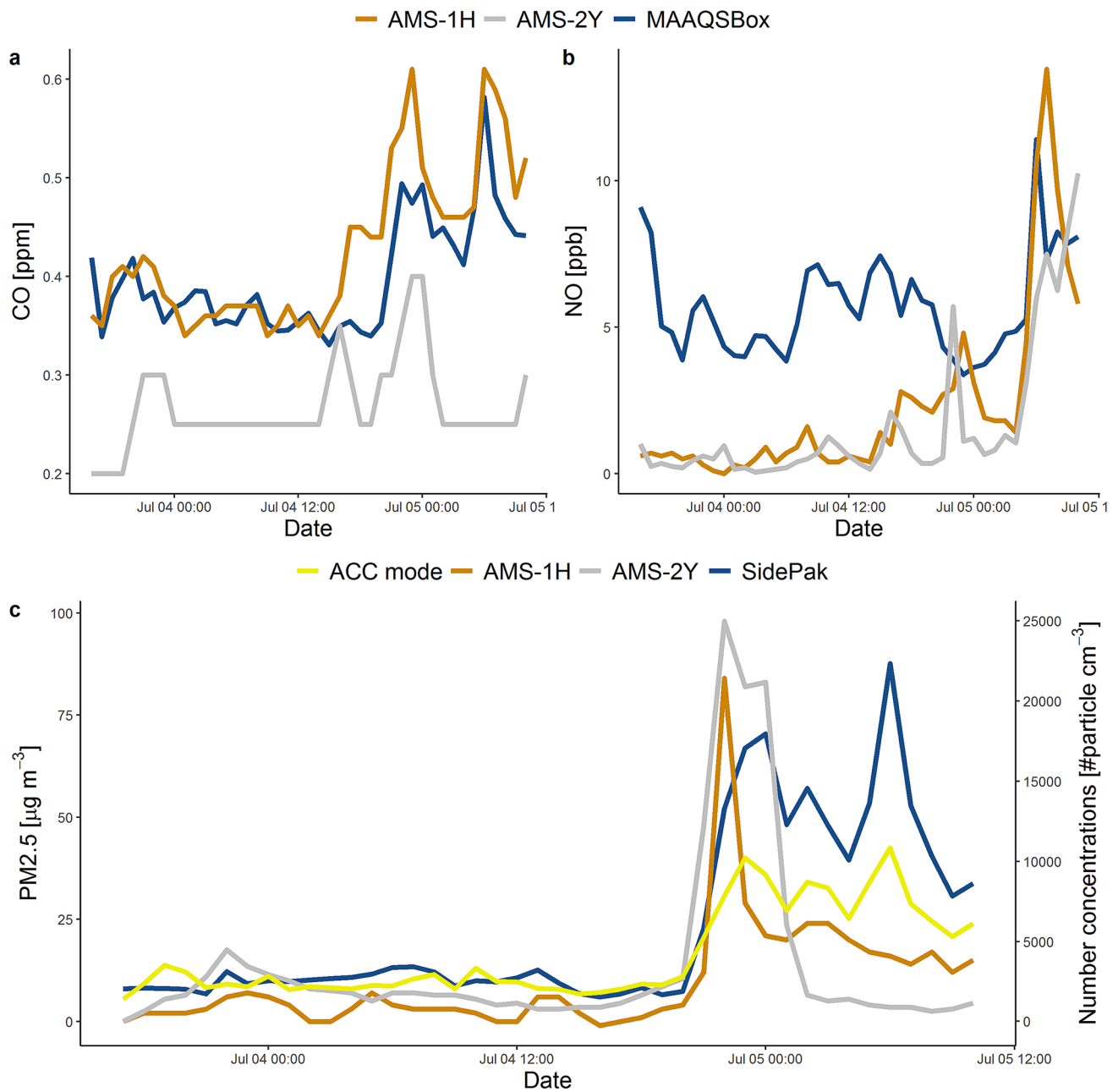


Fig. 6 Fireworks and ambient air quality from July 3rd to 5th July. **a** CO ppm, **b** NO ppb, **c** PM_{2.5} and number. The blue lines represent the data from MAAQSBox, the orange line is the data from AMS during the same time of MAAQSBox measurements (AMS-1H),

and the grey line is the previous 2-years average during same time (AMS-2Y). Yellow line is the accumulation mode number concentration. The data are hourly mean values

profile were also monitored. Concentrations of CO, NO and PM_{2.5} were measured at the AMS. Three measures of particle concentration, particle number, especially in the accumulation mode size range (~50–500 nm diameter), LDSA, and PM_{2.5} all increased significantly because of fireworks. Specifically, between 10 pm and midnight on July 4th, the measures of particle concentration increased by 180–600% compared to the previous night. The concentrations of CO, NO, and CO₂ were less strongly influenced by

fireworks than are particle emissions. Carbon monoxide concentrations were very low and only increased modestly due to the fireworks, increasing from about 0.4 to about 0.5 to 0.6 ppm. Carbon dioxide showed little immediate impact but increased later in the morning due to an inversion. The low-cost NO sensor appeared to malfunction during the fireworks but the NO concentration at the AMS increased from about 1 ppb the previous night to about 5 ppb during the display. All pollutants showed a

secondary peak between about 6 am and 7 am on July 5. The concentrations in the secondary peaks were often as high or higher than in the primary peaks. These peaks are likely due to trapping of pollutants due to low wind speed and a temperature inversion. Particle size distributions measured during rush hour traffic on July 3rd and the morning of July 4th showed the distinct bimodal structure typical of traffic aerosols. However, during and after fireworks the size distribution became nearly unimodal with only a hint of a nucleation mode and a large accumulation mode. This mode was very stable and continued to dominate even during the early morning peak, suggesting that this early morning aerosol consisted mainly of trapped fireworks products.

The low-cost sensors used here showed significant calibration drift so future work should include a more rigorous and frequent calibration routine. Such sensors are developing rapidly, and better performance may be expected of new sensors. Low cost NO₂, SO₂, and PM_{2.5} are now available from several manufacturers. Portable sensor platforms like the MAAQSBox developed here with updated sensors could be usefully deployed for both stationary and mobile air quality measurements.

The particle size distribution measurements were extremely useful and allowed traffic and fireworks emissions to be distinguished easily in real time without the need for chemical analysis. Although particle sizing instruments are not low cost at present, research associated portable emission measurement systems (PEMS) for measuring real-time driving emissions may lead to development of compact lower cost systems.

Acknowledgements This research is supported by University of Minnesota Institute on the Environment. We thank our colleagues from the Department of Civil, Environmental, and Geo- Engineering and the Department of Mechanical Engineering, specially Mugurel Turos and Bernard Olson. We would like also thank Ben Erickson at Saint Anthony Falls Laboratory.

Authors' contribution AG, AB, JS, and DK designed the MAAQSbox. The field measurement was planned by AG and DK and conducted by AG. AG performed the data analysis while the manuscript was prepared with contributions from all co-authors.

Funding The funding source is University of Minnesota by Department of Civil, Environmental, and Geo- Engineering and MnDRIVE Informatics PhD Graduate Assistantships.

Availability of data and material The data are available from Andres Gonzalez (gonza817@umn.edu).

Code availability The data that support the findings of this study are available from the corresponding author upon reasonable request.

Declarations

Conflict of interest Andres Gonzalez declares that he has no conflict of interest. Adam Boies declares that he has no conflict of interest. Jacob Swason declares that he has no conflict of interest. David Kitelson declares that he has no conflict of interest.

Ethical approval This article does not contain any studies with human participants or animals performed by any of the authors.

Open Access This article is licensed under a Creative Commons Attribution 4.0 International License, which permits use, sharing, adaptation, distribution and reproduction in any medium or format, as long as you give appropriate credit to the original author(s) and the source, provide a link to the Creative Commons licence, and indicate if changes were made. The images or other third party material in this article are included in the article's Creative Commons licence, unless indicated otherwise in a credit line to the material. If material is not included in the article's Creative Commons licence and your intended use is not permitted by statutory regulation or exceeds the permitted use, you will need to obtain permission directly from the copyright holder. To view a copy of this licence, visit <http://creativecommons.org/licenses/by/4.0/>.

References

1. Lai Y, Brimblecombe P (2020) Changes in air pollution and attitude to fireworks in Beijing. *Atmos Environ* 231:117549. <https://doi.org/10.1016/j.atmosenv.2020.117549>
2. Kumar P, Gupta NC (2018) Firework-induced particulate and heavy metal emissions during the Diwali festival in Delhi, India. (International Perspectives). *J Environ Health* 81(4):E1–E1. <https://doi.org/10.30852/sb.2019.799>
3. Pope RJ, Marshall AM, O'Kane BO (2016) Observing UK bonfire night pollution from space: analysis of atmospheric aerosol. *Weather* 71(11):288–291. <https://doi.org/10.1002/wea.2914>
4. Yao L, Wang D, Fu Q, Qiao L, Wang H, Li L, Zhao Z (2019) The effects of firework regulation on air quality and public health during the Chinese spring festival from 2013 to 2017 in a Chinese megacity. *Environ Int* 126:96–106. <https://doi.org/10.1016/j.envint.2019.01.037>
5. Zhang Y, Wei J, Tang A, Zheng A, Shao Z, Liu X (2017) Chemical characteristics of PM_{2.5} during 2015 spring festival in Beijing China. *Aerosol Air Qual Res* 17(5):1169–1180. <https://doi.org/10.4209/aaqr.2016.08.0338>
6. Rindelaub JD, Davy PK, Talbot N, Pattinson W, Miskelly GM (2021) The contribution of commercial fireworks to both local and personal air quality in Auckland, New Zealand. *Environ Sci Pollut Res* 28(17):21650–21660. <https://doi.org/10.1007/s11356-020-11889-4>
7. Greven FE, Vonk JM, Fischer P, Duijm F, Vink NM, Brunekreef B (2019) Air pollution during New Year's fireworks and daily mortality in the Netherlands. *Sci Rep* 9(1):5735. <https://doi.org/10.1038/s41598-019-42080-6>
8. Seidel DJ, Birnbaum AN (2015) Effects of Independence Day fireworks on atmospheric concentrations of fine particulate matter in the United States. *Atmos Environ* 115:192–198. <https://doi.org/10.1016/j.atmosenv.2015.05.065>
9. Zhang M, Wang X, Chen J, Cheng T, Wang T, Yang X, Chen C (2010) Physical characterization of aerosol particles during the Chinese New Year's firework events. *Atmos Environ* 44(39):5191–5198. <https://doi.org/10.1016/j.atmosenv.2010.08.048>

10. Hamad S, Green D, Heo J (2016) Evaluation of health risk associated with fireworks activity at Central London. *Air Qual Atmos Health* 9(7):735–741. <https://doi.org/10.1007/s11869-015-0384-x>
11. Hirai K, Yamazaki Y, Okada K, FURUTA S, KUBO K (2000) Acute eosinophilic pneumonia associated with smoke from fireworks. *Intern Med* 39(5):401–403. <https://doi.org/10.2169/internalmedicine.39.401>
12. Sharma S, Nayak H, Lal P (2015) Post-Diwali morbidity survey in a resettlement colony of Delhi. *Indian J Burns* 23(1):76. <https://doi.org/10.4103/0971-653X.171662>
13. Yerramsetti VS, Sharma AR, Navlur NG, Rapolu V, Dhulipala NC, Sinha PR (2013) The impact assessment of Diwali fireworks emissions on the air quality of a tropical urban site, Hyderabad, India, during three consecutive years. *Environ Monit Assess* 185(9):7309–7325. <https://doi.org/10.1007/s10661-013-3102-x>
14. Barman SC, Singh R, Negi MPS, Bhargava SK (2008) Ambient air quality of Lucknow City (India) during use of fireworks on Diwali Festival. *Environ Monit Assess* 137(1–3):495–504. <https://doi.org/10.1007/s10661-007-9784-1>
15. Ravindra K, Mor S, Kaushik CP (2003) Short-term variation in air quality associated with firework events: a case study. *J Environ Monit* 5(2):260–264. <https://doi.org/10.1039/B211943A>
16. Yadav SK, Kumar M, Sharma Y, Shukla P, Singh RS, Banerjee T (2019) Temporal evolution of submicron particles during extreme fireworks. *Environ Monit Assess* 191(9):576. <https://doi.org/10.1007/s10661-019-7735-2>
17. Caudillo L, Salcedo D, Peralta O, Castro T, Alvarez-Ospina H (2020) Nanoparticle size distributions in Mexico City. *Atmos Pollut Res* 11(1):78–84. <https://doi.org/10.1016/j.apr.2019.09.017>
18. Dickerson AS, Benson AF, Buckley B, Chan EA (2017) Concentrations of individual fine particulate matter components in the USA around July 4th. *Air Qual Atmos Health* 10(3):349–358. <https://doi.org/10.1007/s11869-016-0433-0>
19. Gonzalez A, Boies A, Swanson J, Kittelson D (2019) Measuring the effect of ventilation on cooking in indoor air quality by low-cost air sensors. *Int J Environ Ecol Eng* 13(9):568–576. <https://doi.org/10.5281/zenodo.3455739>
20. Castell N, Dauge FR, Schneider P, Vogt M, Lerner U, Fishbain B, Bartonova A (2017) Can commercial low-cost sensor platforms contribute to air quality monitoring and exposure estimates? *Environ Int* 99:293–302. <https://doi.org/10.1016/j.envint.2016.12.007>
21. Mijling B, Jiang Q, de Jonge D, Bocconi S (2017) Practical field calibration of electrochemical NO₂ sensors for urban air quality applications.
22. Wilson WE, Stanek J, Han HS, Johnson T, Sakurai H, Pui DY, Duthie S (2007) Use of the electrical aerosol detector as an indicator of the surface area of fine particles deposited in the lung. *J Air Waste Manag Assoc* 57(2):211–220. <https://doi.org/10.1080/10473289.2007.10465321>
23. Fierz M, Houle C, Steigmeier P, Burtscher H (2011) Design, calibration, and field performance of a miniature diffusion size classifier. *Aerosol Sci Technol* 45(1):1–10. <https://doi.org/10.1080/02786826.2010.516283>
24. Baron R, Saffell J (2017) Amperometric gas sensors as a low cost emerging technology platform for air quality monitoring applications: a review. *ACS Sens* 2(11):1553–1566. <https://doi.org/10.1021/acssensors.7b00620>
25. Spinelle L, Gerboles M, Villani MG, Alexandre M, Bonavitacola F (2015) Field calibration of a cluster of low-cost available sensors for air quality monitoring. Part A: ozone and nitrogen dioxide. *Sens Actuators B Chem* 215:249–257. <https://doi.org/10.1016/j.snb.2015.03.031>
26. Wilson D, Phair JW, Lengden M (2019) Performance analysis of a novel pyroelectric device for non-dispersive infra-red CO₂ detection. *IEEE Sens J* 19(15):6006–6011. <https://doi.org/10.1109/JSEN.2019.2911737>
27. Martin CR, Zeng N, Karion A, Dickerson RR, Ren X, Turpie BN, Weber KJ (2017) Evaluation and environmental correction of ambient CO₂ measurements from a low-cost NDIR sensor. *Atmos Meas Tech* 10(7):2383–2395. <https://doi.org/10.5194/amt-10-2383-2017>
28. Fierz M, Meier D, Steigmeier P, Burtscher H (2015) Miniature nanoparticle sensors for exposure measurement and TEM sampling. In: *Journal of Physics: Conference Series*. 617(1): 012034. IOP Publishing
29. Kuula J, Kuuluvainen H, Rönkkö T, Niemi JV, Saukko E, Portin H, Timonen H (2019) Applicability of optical and diffusion charging-based particulate matter sensors to urban air quality measurements. *Aerosol Air Qual Res* 19(5):1024–1039. <https://doi.org/10.4209/aaqr.2018.04.0143>
30. TSI SidePak Personal Aerosol Monitor AM510 (2019) <https://www.tsi.com/discontinued-products/sidepak-personal-aerosol-monitor-am510/> (Accessed on 9 May 2019)
31. Jiang RT, Acevedo-Bolton V, Cheng KC, Klepeis NE, Ott WR, Hildemann LM (2011) Determination of response of real-time SidePak AM510 monitor to secondhand smoke, other common indoor aerosols, and outdoor aerosol. *J Environ Monit* 13(6):1695–1702. <https://doi.org/10.1039/C0EM00732C>
32. Christiani DC (2009) Association between fine particulate matter and oxidative DNA damage may be modified in individuals with hypertension. *J occup environ med Am Coll Occup Environ Med* 51(10):1158. <https://doi.org/10.1097/JOM.0b013e3181b967aa>
33. Wang Y, Li J, Jing H, Zhang Q, Jiang J, Biswas P (2015) Laboratory evaluation and calibration of three low-cost particle sensors for particulate matter measurement. *Aerosol Sci Technol* 49(11):1063–1077. <https://doi.org/10.1080/02786826.2015.1100710>
34. Tritscher T, Zerrath AF, Elzey S, Han HS (2013) Data merging of size distributions from electrical mobility and optical measurements. *Technology* 38(12):1185–1205
35. TSI NanoScan SMPS (2012). Particle Instruments. Specifications NanoScan SMPS Model 3910
36. Yamada M, Takaya M, Ogura I (2015) Performance evaluation of newly developed portable aerosol sizers used for nanomaterial aerosol measurements. *Ind Health* 53:511–516
37. Xiang J, Austin E, Gould T, Larson T, Shirai J, Liu Y, Seto E (2020) Impacts of the COVID-19 responses on traffic-related air pollution in a Northwestern US city. *Sci Total Environ* 747(2020):141325. <https://doi.org/10.1016/j.scitotenv.2020.141325>
38. Zhang Y (2019) Dynamic effect analysis of meteorological conditions on air pollution: a case study from Beijing. *Sci Total Environ* 684:178–185. <https://doi.org/10.1016/j.scitotenv.2019.05.360>
39. Coccia M (2021) The effects of atmospheric stability with low wind speed and of air pollution on the accelerated transmission dynamics of COVID-19. *Int J Environ Stud* 78(1):1–27. <https://doi.org/10.1080/00207233.2020.1802937>
40. Hilker N, Wang JM, Jeong CH, Healy RM, Sofowote U, Deboz J, Evans GJ (2019) Traffic-related air pollution near roadways: discerning local impacts from background. *Atmos Meas Technol* 12(10):5247–5261. <https://doi.org/10.5194/amt-12-5247-2019>
41. Trinh TT, Le TT, Tu BM (2019) Temperature inversion and air pollution relationship, and its effects on human health in Hanoi City. *Vietnam Environ geochem health* 41(2):929–937. <https://doi.org/10.1007/s10653-018-0190-0>
42. Jury MR (2020) Meteorology of air pollution in Los Angeles. *Atmos Pollut Res* 11(7):1226–1237. <https://doi.org/10.1016/j.apr.2020.04.016>
43. Qiu H, Yu ITS, Wang X, Tian L, Tse LA, Wong TW (2013) Season and humidity dependence of the effects of air pollution on COPD

- hospitalizations in Hong Kong. *Atmos Environ* 76:74–80. <https://doi.org/10.1016/j.atmosenv.2012.07.026>
44. Slezakova K, Pires JCM, Castro D, Alvim-Ferraz M, Delerue-Matos C, Morais S, Pereira MDC (2013) PAH air pollution at a Portuguese urban area: carcinogenic risks and sources identification. *Environ Sci Pollut Res* 20(6):3932–3945. <https://doi.org/10.1007/s11356-012-1300-7>
 45. Han B, Wang Y, Zhang R, Yang W, Ma Z, Geng W, Bai Z (2019) Comparative statistical models for estimating potential roles of relative humidity and temperature on the concentrations of secondary inorganic aerosol: statistical insights on air pollution episodes at Beijing during January 2013. *Atmos Environ* 212:11–21. <https://doi.org/10.1016/j.atmosenv.2019.05.025>
 46. Sun Y, Wang Z, Fu P, Jiang Q, Yang T, Li J, Ge X (2013) The impact of relative humidity on aerosol composition and evolution processes during wintertime in Beijing, China. *Atmos Environ* 77:927–934. <https://doi.org/10.1016/j.atmosenv.2013.06.019>
 47. Nemitz E, Hargreaves KJ, McDonald AG, Dorsey JR, Fowler D (2002) Micrometeorological measurements of the urban heat budget and CO₂ emissions on a city scale. *Environ Sci Technol* 36(14):3139–3146. <https://doi.org/10.1021/es010277e>
 48. Nasrallah HA, Balling RC Jr, Madi SM, Al-Ansari L (2003) Temporal variations in atmospheric CO₂ concentrations in Kuwait City, Kuwait with comparisons to Phoenix, Arizona, USA. *Environ Pollut* 121(2):301–305. [https://doi.org/10.1016/S0269-7491\(02\)00221-X](https://doi.org/10.1016/S0269-7491(02)00221-X)
 49. Belikov D, Arshinov M, Belan B, Davydov D, Fofonov A, Sasakawa M, Machida T (2019) Analysis of the diurnal, weekly, and seasonal cycles and annual trends in atmospheric CO₂ and CH₄ at Tower Network in Siberia from 2005 to 2016. *Atmosphere* 10(11):689. <https://doi.org/10.3390/atmos10110689>
 50. Cheng XL, Liu XM, Liu YJ, Hu F (2018) Characteristics of CO₂ concentration and flux in the Beijing urban area. *J Geophys Res Atmos* 123(3):1785–1801. <https://doi.org/10.1002/2017JD027409>
 51. Hernández-Paniagua IY, Lowry D, Clemitshaw KC, Fisher RE, France JL, Lanoisellé M, Nisbet EG (2015) Diurnal, seasonal, and annual trends in atmospheric CO₂ at southwest London during 2000–2012: wind sector analysis and comparison with Mace Head, Ireland. *Atmos Environ* 105:138–147. <https://doi.org/10.1016/j.atmosenv.2015.01.021>
 52. Imasu R, Tanabe Y (2018) Diurnal and seasonal variations of carbon dioxide (CO₂) concentration in urban, suburban, and rural areas around Tokyo. *Atmosphere* 9(10):367. <https://doi.org/10.3390/atmos9100367>
 53. Wang Y, Wang C, Guo X, Liu G, Huang Y (2002) Trend, seasonal and diurnal variations of atmospheric CO₂ in Beijing. *Chin Sci Bull* 47(24):2050–2055. <https://doi.org/10.1360/02tb9444>
 54. Yuan Y, Ries L, Petermeier H, Trickl T, Leuchner M, Couret C, Menzel A (2019) On the diurnal, weekly, and seasonal cycles and annual trends in atmospheric CO₂ at Mount Zugspitze, Germany, during 1981–2016. *Atmos Chem Phys* 19(2):999–1012. <https://doi.org/10.5194/acp-19-999-2019>
 55. Pan C, Zhu X, Wei N, Zhu X, She Q, Jia W, Xiang W (2016) Spatial variability of daytime CO₂ concentration with landscape structure across urbanization gradients, Shanghai. *China Clim Res* 69(2):107–116. <https://doi.org/10.3354/cr01394>
 56. Kittelson D, Khalek I, McDonald J, Stevens J, Giannelli R (2022) Particle emissions from mobile sources: discussion of ultrafine particle emissions and definition. *J Aerosol Sci* 159:105881. <https://doi.org/10.1016/j.jaerosci.2021.105881>
 57. Joshi M, Nakhwa A, Khandare P, Khan A, Sapra BK (2019) Simultaneous measurements of mass, chemical compositional and number characteristics of aerosol particles emitted during fireworks. *Atmos Environ* 217:116925. <https://doi.org/10.1016/j.atmosenv.2019.116925>
 58. Chang PK, Griffith SM, Chuang HC, Chuang KJ, Wang YH, Chang KE, Hsiao TC (2021) Particulate matter in a motorcycle-dominated urban area: source apportionment and cancer risk of lung deposited surface area (LDSA) concentrations. *J Hazard Mater*. <https://doi.org/10.1016/j.jhazmat.2021.128188>
 59. Schneider IL, Teixeira EC, Oliveira LFS, Wiegand F (2015) Atmospheric particle number concentration and size distribution in a traffic-impacted area. *Atmos Pollut Res* 6(5):877–885. <https://doi.org/10.5094/APR.2015.097>
 60. EPA U (2004) Air quality criteria for particulate matter (Final Report, Oct 2004). Environmental Protection Agency, Washington, DC
 61. Kittelson DB (1998) Engines and nanoparticles: a review. *J Aerosol Sci* 29(5–6):575–588. [https://doi.org/10.1016/S0021-8502\(97\)10037-4](https://doi.org/10.1016/S0021-8502(97)10037-4)
 62. Whitby KT (1978) The physical characteristics of sulfur aerosols. In *Sulfur in the Atmosphere*. doi: <https://doi.org/10.1016/B978-0-08-022932-4.50018-5>
 63. Kittelson D, Kraft M (2015) Particle formation and models. In: Crolla D, Foster DE, Kobayashi T, Vaughan N (eds) *Encyclopedia of automotive engineering*. John Wiley & Sons Ltd, Chichester, pp 107–130
 64. Wehner B, Wiedensohler A, Heintzenberg J (2000) Submicrometer aerosol size distributions and mass concentration of the millennium fireworks 2000 in Leipzig. *Ger J Aerosol Sci* 12(31):1489–1493. [https://doi.org/10.1016/S0021-8502\(00\)00039-2](https://doi.org/10.1016/S0021-8502(00)00039-2)
 65. Al-Dabbous AN, Kumar P (2015) Source apportionment of airborne nanoparticles in a middle eastern city using positive matrix factorization. *Environ Sci Process Impacts* 17(4):802–812. <https://doi.org/10.1039/C5EM00027K>
 66. Belkacem I, Khardi S, Helali A, Slimi K, Serindat S (2020) The influence of urban road traffic on nanoparticles: roadside measurements. *Atmos Environ* 242:117786. <https://doi.org/10.1016/j.atmosenv.2020.117786>
 67. Masiol M, Harrison RM, Vu TV, Beddows D (2017) Sources of submicrometre particles near a major international airport. *Atmos Chem Phys* 17(20):12379–12403. <https://doi.org/10.5194/acp-17-12379-2017>
 68. Deventer MJ, von der Heyden L, Lamprecht C, Graus M, Karl T, Held A (2018) Aerosol particles during the innsbruck air quality study (INNAQS): fluxes of nucleation to accumulation mode particles in relation to selective urban tracers. *Atmos Environ* 190:376–388. <https://doi.org/10.1016/j.atmosenv.2018.04.043>
 69. Zhong J, Nikolova I, Cai X, MacKenzie AR, Harrison RM (2018) Modelling traffic-induced multicomponent ultrafine particles in urban street canyon compartments: factors that inhibit mixing. *Environ Pollut* 238:186–195. <https://doi.org/10.1016/j.envpol.2018.03.002>
 70. Li J, Xu T, Lu X, Chen H, Nizkorodov SA, Chen J, Liang G (2017) Online single particle measurement of fireworks pollution during Chinese New Year in Nanning. *J Environ Sci* 53:184–195. <https://doi.org/10.1016/j.jes.2016.04.021>
 71. Tanda S, Ličbinský R, Hegrová J, Goessler W (2019) Impact of New Year's Eve fireworks on the size resolved element distributions in airborne particles. *Environ Int* 128:371–378. <https://doi.org/10.1016/j.envint.2019.04.071>
 72. Gautam S, Yadav A, Pillarisetti A, Smith K, Arora N (2018) Short-term introduction of air pollutants from fireworks during Diwali in rural Palwal, Haryana, India: a case study. In: *IOP Conference Series: Earth and Environmental Science* 120(1):012009. IOP

Publishing. doi:<https://doi.org/10.1088/1755-1315/120/1/012009/meta>

73. Rim-Rukeh A (2019) Effects of New Year Eve's fireworks on the ambient air quality in Woji community, Port Harcourt, Nigeria. *FUPRE J Sci Ind Res (FJSIR)* 3(1):29–45
74. Subhashini R, Samhitha BK, Mana SC, Jose J (2019) Data analytics to find out the effect of firework emissions on quality of air: a case study. In: *AIP Conference Proceedings* 2201(1): 020008. AIP Publishing LLC. doi:<https://doi.org/10.1063/1.5141432>

Publisher's Note Springer Nature remains neutral with regard to jurisdictional claims in published maps and institutional affiliations.